Short and long-term prestress losses in basalt FRP prestressed concrete beams under sustained loading

Ana Pavlović[1], Ted Donchev[2], Diana Petkova[3], Mukesh Limbachiya[4],

[1] *Ph.D. Candidate, Dept. of Civil Engineering, Surveying and Construction Management, Kingston Univ., Penrhyn Rd., Kingston upon Thames KT1 2EE, UK. Email: ana.pavlovic.grf@gmail.com*

[2] *Associate Professor, Dept. of Civil Engineering, Surveying and Construction Management, Kingston Univ., Penrhyn Rd., Kingston upon Thames KT1 2EE, UK. Email: t.donchev@kingston.ac.uk*

[3] *Senior Lecturer, Dept. of Civil Engineering, Surveying and Construction Management, Kingston Univ., Penrhyn Rd., Kingston upon Thames KT1 2EE, UK. Email: d.petkova@kingston.ac.uk*

[4] *Professor, Dept. of Civil Engineering, Surveying and Construction Management, Kingston Univ., Penrhyn Rd., Kingston upon Thames KT1 2EE, UK.*

Abstract

The favourable mechanical properties of basalt fibre-reinforced polymer (BFRP) bars, such as their excellent strength-to-weight ratio, resistance to corrosion, lower environmental impact and electro-magnetic neutrality, make them attractive for internal reinforcement of concrete elements with specific service requirements. Prestressing has emerged as a possible method for limiting the deflections and cracking of BFRP reinforced flexural RC elements. However, long-term behaviour of such structural members has not yet been investigated extensively. Therefore, this paper aims to give information on long-term behaviour and prestress losses of pretensioned BFRP reinforced concrete beams based on the collected experimental data. The testing programme includes long-term analysis of six BFRP concrete beams pretensioned to different prestress levels; namely, 20%, 30% and 40% of the ultimate tensile capacity of the bars. The monitored testing stages included initial tensioning of the bars, casting and curing of concrete, transfer of prestressing force to the concrete, long-term unloaded phase after transfer, sustained loading application, long-term sustained loading phase, unloading and final destructive testing, conducted in a controlled indoor environment. During all phases of the testing strain levels in the BFRP bars and deflections were continuously monitored. The results of continuous strain monitoring show that the average loss of strain over the period of initial 90 days of

unloaded monitoring was 7% of the initial strain. During the following 6 months of monitoring under sustained loading recorded an additional 0.3% reduction on average. The loss was dependent on the initial strain.

Keywords: prestress losses, BFRP, long-term, FRP internal reinforcement, PT RC beams.

Background

One of the suitable solutions for meeting the design requirements and overcoming the issues primarily related to steel corrosion in aggressive environments can be seen in the use of fibre reinforced polymers. Favourable properties of fibre-reinforced polymer (FRP) materials, such as their low density, high tensile capacity, corrosion resistance etc. have made these composites attractive, despite the slightly higher manufacturing cost, due to their lifecycle advantages. The most commonly used types are carbon FRP (CFRP) and glass FRP (GFRP). More recently, basalt FRP (BFRP) has attracted attention. Similarly to GFRP, BFRP reinforcement is more economically competitive than CFRP for structural applications (Zoghi 2013; Kim et al. 2014) (Zoghi 2013; Kim et al. 2014) . The interest in BFRP emerged due to widespread availability of the raw material used for production of fibres, lower environmental impact (Inman et al. 2017; Pavlović et al. 2022)(Inman et al. 2017), as well as comparable or superior mechanical properties to those of GFRP (Wei et al. 2011)(Wei et al. 2011). However, due to the inherent material properties variability of basalt fibres due to their natural origin, or variation of manufacturing process (Atutis et al., 2018a) a larger variation of basalt composite mechanical properties is possible. This can be remedied employing a conservative engineering approach of utilising nominal strength values at the lower boundary of variation.

Up to date, applications for BFRP include structural strengthening (Jason et al. 2018; Suon et al. 2019; He et al. 2020; Hou et al. 2020; Madotto et al. 2021)(Jason et al. 2018; Suon et al. 2019; He et al. 2020; Hou et al. 2020; Madotto et al. 2021), reinforcing for buried utility tunnels (Meng et al. 2020; Zhou et al. 2021)(Meng et al. 2020; Zhou et al. 2021), flexural elements (Crossett et al. 2015; Douglas and Amir 2015; Dal Lago et al. 2017; Younes et al. 2017; Attia et al. 2020)(Crossett et al. 2015; Douglas and Amir 2015; Dal Lago et al. 2017; Younes et al. 2017; Attia et al. 2020) and offshore platforms (Younes et al. 2017; Atutis et al. 2019), to name a few. Investigating the bond durability of BFRP bars in concrete has shown their suitability as an alternative to GFRP as internal reinforcement (Ahmed et al. 2015)(Ahmed et al. 2015), although a reduction in bond retention has been noted for BFRP bars embedded in seawater sea-sand concrete (SWSSC) in marine environment (Zhi-Qiang et al. 2018)(Zhi-Qiang et al. 2018).

The determination of mechanical properties and performance of BFRP under different environmental conditions and the understanding of corrosion mechanisms is important for the correct prediction of the service life. The material possesses a significantly higher tensile capacity than reinforcing steel, better insulating properties, as well as more economic manufacturing process compared to CFRP and GFRP (Czigány 2005; Scheffler et al. 2009; Wei et al. 2010; Singha 2012; Dhand et al. 2015)(Czigány 2005; Scheffler et al. 2009; Wei et al. 2010; Singha 2012; Dhand et al. 2015). The blast resilience of BFRP reinforced elements is also excellent due to the high deformability of the reinforcement (Feng et al. 2017; Gao et al. 2020)(Feng et al. 2017; Gao et al. 2020). It has been demonstrated that BFRP has good resistance to acidic environments (Wu et al. 2014; Gang et al. 2015; Li et al. 2016)(Wu et al. 2014; Gang et al. 2015; Li et al. 2016), and high resistance to both simulated and real marine environments (Gang et al. 2015; Lu et al. 2020)(Gang et al. 2015; Lu et al. 2020). Alkali resistance has also been investigated by Gang et al. (2015)Gang et al. (2015), noting the simultaneous influence of temperature and stress level on the degradation of the capacity of BFRP bars.

One of the main issues regarding the use of FRPs with low longitudinal elastic modulus, such as GFRP and BFRP, as internal reinforcement of flexural elements, are the large deflections occurring at relatively low levels of load. This leads to a poor utilisation of the FRPs' tensile capacity, as designers are forced to increase the reinforcement ratio to satisfy the serviceability limit state (SLS) criteria. To improve the efficiency of the design, prestressing of reinforcement has been adopted as an effective approach in previous research (Thorhallsson et al. 2012; Pearson and Donchev, 2013; Thorhallsson and Gudmundsson, 2013; Mirshekari et al., 2015; Mirshekari et al., 2016)(Thorhallsson et al. 2012; Pearson and Donchev, 2013; Thorhallsson and Gudmundsson, 2013; Mirshekari et al., 2015;

Mirshekari et al., 2016). The evidence shows that prestressed BFRP reinforced elements have improved stiffness, approaching or surpassing that of steel reinforced elements with the same reinforcement ratio at levels of prestress over 30% of the ultimate tensile capacity of the bars. Due to the anisotropy of the mechanical properties of BFRP, the anchorage of tendons is also an area of high importance, especially for prestressing applications; issues such as slipping or crushing of the tendons have been reported when using industrial wedge anchorage (Dal Lago et al. 2017; Motwani et al. 2020)(Dal Lago et al. 2017; Motwani et al. 2020).

GFRP has been used in prestressing in the form of E-glass and polyester resin bars, E-glass and vinylester resin bars and S-glass and epoxy strands (Rossini and Nanni, 2019). Prestressed beams were tested by Atutis, Valivonis and Atutis (2015) and Zawam, Soudki and West (2019) with prestressing levels of 27% and 25% and 40% of the ultimate guaranteed strength respectively. Rossini and Nanni (2019) concluded that GFRP strands could be used with traditional steel anchors in design of elements prestressed to about 40% of the guaranteed tensile strength.

The losses of prestress due to creep and stress relaxation were also reported. Zawam, Soudki and West (2019 observed no relaxation for the first 277h for GFRP bars made of continuous glass fibres impregnated in Vinyl-Ester resin. Nkurunziz et al. (2005) tested GFRP bars made of high strength E-glass fibres with vinylester resin in alkaline conditions and de-ionised water and stressed to 25 and 38% of the guaranteed tensile strength. The creep test based on 10000h revealed strain increase of 3% for 25% level of prestress and 5% for 38% prestress. Elevated temperature of 60°C caused strain increase of 8% after 114 days for 38% prestress.

A smaller number of studies to date has focused on time-dependent properties of the BFRP material and long-term performance. The fatigue performance of BFRP bars in the context of potential application as prestressing tendons has been investigated in (Xin et al. 2016)(Xin et al. 2016), recommending a limit of stress range of 4% f_{tu} and maximum stress of 53% f_{tu} for BFRP bars. In a study of prestressed concrete beams with BFRP bars, Atutis et al. (2018a) concluded that the stress range varying between 55% and 65% f_{tu} can be considered as safe for BFRP bars.

Creep behaviour of BFRP has been investigated in (Wang et al. 2014; Sokairge et al. 2020)(Wang et al. 2014; Sokairge et al. 2020), estimating the million-hour creep rupture stress limit between 57.7% and 62.3%. These values can reportedly be improved to up to 63% by preconditioning of the bars via pretensioning for a short duration (Shi et al. 2015)(Shi et al. 2015). A similar conclusion about the reduction of creep rate by short-term pretensioning of bars at low levels of stress, has been demonstrated in a study of creep at low levels of stress, up to 40% f_{tu} (Pavlović et al., 2021), observing also a stabilisation of the deformation after a relatively short time interval. Stress relaxation has been shown experimentally to depend on the initially applied stress, with measured 1000-hour relaxation of close to 6% (Atutis et al. 2018b).(Atutis et al. 2018b).

However, long-term behaviour of pretensioned BFRP reinforced concrete elements is insufficiently investigated to date, in particular regarding losses of prestress. The current structural design codes do not provide clear guidance for the calculation of this fundamental design parameter. Information about the prestress losses is also very limited in the available published research, both from experimental (Pavlović et al. 2019b)(Pavlović et al. 2019b) and numerical studies (Atutis and Kawashima 2020)(Atutis and Kawashima 2020). Hence, this paper aims to experimentally investigate the losses of prestress as well as flexural behaviour of pretensioned BFRP reinforced concrete beams via long-term monitoring.

Methodology

Samples

The experimental study was based on the investigation of six concrete beam samples. All beams were 1200 mm long with a cross section of 130x180 mm. The main (tensile) reinforcement consisted of two 6 mm diameter BFRP bars. The BFRP bars used in this experiment were straight pultruded bars, with surface sand coating, 85_{wt}% fibre fraction (by weight) and epoxy resin. The nominal diameter of 6 mm was used in all calculations; the measured diameter was 6.84 mm (standard deviation 0.04 mm) including the sand coating, while the measured diameter after removal of the sand coating was 6.00 mm (standard deviation 0.01 mm). The reported measured values were based on average of 5 readings taken using a digital calliper with 0.01 mm precision, as shown in Figure 1. They were characterised by average ultimate tensile capacity of f_{tu}=1278 MPa (standard deviation 84 MPa) and longitudinal elastic modulus of E=48 GPa (standard deviation 1.4 GPa); this was experimentally determined on a sample of 9 bars, following the procedure given in ASTM D7205/D7205M (ASTM, 2016) for tensile testing of FRP. Ultimate tensile capacity was adopted as 1200 MPa for the purpose of all calculations in this paper, which agrees also with the reported minimum capacity provided by the manufacturer.

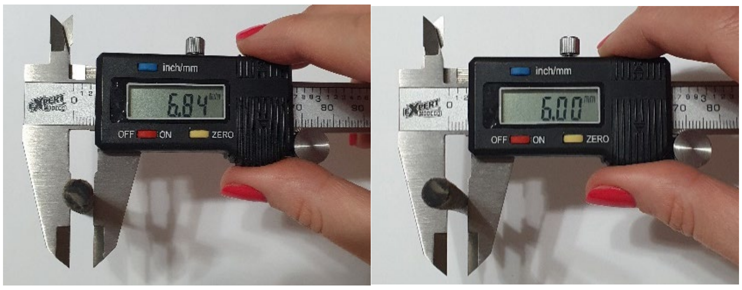

Figure 1 Measurement of the BFRP bar cross section diameter with (left) and without (right) sand coating

In addition, 6 mm S275 links were used to prevent shear failure, except in the pure bending zone (middle 300 mm). Top reinforcement of two 6 mm diameter S375 steel bars was also used to construct the reinforcement cage. The top bars were not designed as compression reinforcement due to the expected mode of failure governed by rupture of the bottom BFRP bars, and were provided to keep the shear reinforcement in the correct position.

The ends of the BFRP bars were connected to threaded steel bars via bonded steel sleeve anchorage (Figure 2), in accordance with the recommendations given in ASTM D7205/D7205M (ASTM, 2016), prepared using Weber.tec epoxy structural adhesive. The adhesive was cured at room temperature (20°C) for a minimum of 24h in line with manufacturers guidelines. The threaded steel bars were tensioned using a manual hydraulic ram until the desired prestress level was achieved and then mechanically fastened to steel angle sections securely bolted into the reaction floor. All samples were produced in specially prepared formwork with a divider in the middle, which allowed for simultaneous prestressing of two beams.

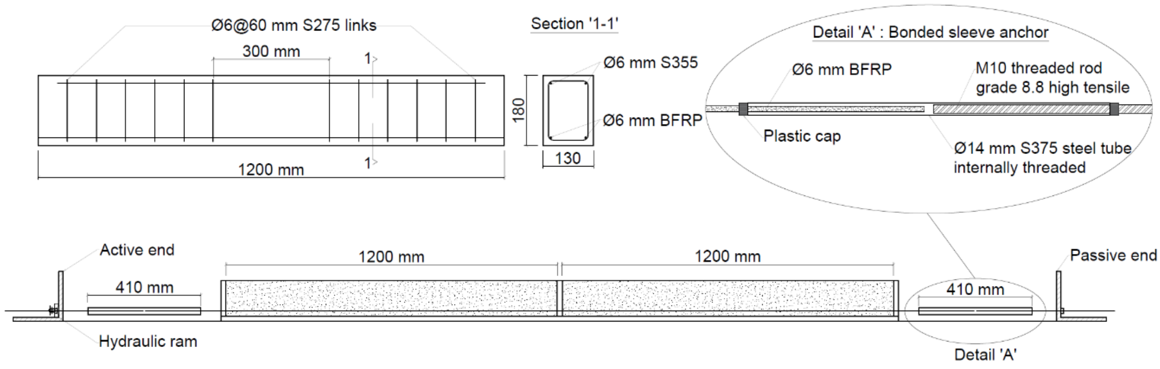

Figure 2 Sample dimensions and prestressing setup

After the pretensioning of the bars was completed, all beams were cast using the same concrete mix (1238 kg/m^3 coarse aggregate, 583 kg/m^3 fine aggregate, 180 kg/m^3 water, 379 kg/m^3 cement). The curing was done in laboratory conditions for 28 days, after which the threaded bars were released from the steel angles and the prestress force transferred to the concrete samples. The pairs of samples were separated by carefully cutting the BFRP bars between them.

The samples were cured in controlled indoor laboratory conditions, preventing loss of moisture by regular spraying of water and provided damp covering sheets. After 28 days curing of the concrete, the prestress was gradually released from the external anchorage and transferred to concrete by unscrewing the anchor nuts, whilst clamping the anchor sleeves to prevent torsional effects. The compressive strength of concrete was tested on the day of prestress transfer, according to BS EN 12390-3:2002 (BSI, 2002). The average of 42 MPa cube strength was obtained on a sample of nine 150 mm cubes, with coefficient of variation CV=4.5%.

Testing programme

After the release of the prestress, the strain of the BFRP bars was monitored for three months in unloaded conditions. Then, the samples were loaded using the testing rig (Figure 3), based on gravitational load and lever-arm principle, with the aim of maintaining a constant load over a prolonged period of time. The static system corresponds to four-point bending, over a span of 900 mm and 300 mm distance between the point loads.

Figure 3. Samples in the sustained loading testing rig

The load was applied gradually in steps of approximately 1.5 kN up to the planned level and maintained for 6 months. The samples were subjected to two different levels of loading: 10 kN and 14.5 kN as total values monitored by the load cells. The load values were chosen as approximately 20% and 30% of the predicted ultimate capacity of the beams, estimated using fib model code EC2 based approach for FRP reinforced elements. These values are approximately representative of the permanent service loads for building structures. Both of the loads were below the cracking load estimated using the Response2000 software (Bentz, 2000) as presented in Table 2.

The following alphanumerical labelling system was adopted for all samples: Bnα-Lβ; where n={20; 30; 40} depending on the degree of prestress as a percentage of the ultimate tensile capacity of the bars, α={A; P} depending on whether the beams was cast at the active (A) or passive (P) end of the prestressing rig (see Figure 2), and β={10; 14.5} depending on the level of externally applied load in kN. The difference between the samples cast at the active (A) or passive (P) end was due to the friction inside the formwork, as the cages and the formwork were assembled prior to the tensioning process. Table 1 details the sample matrix:

Table 1. Sample matrix

Sample	**Prestress level [%f_{tu}]**	**Applied sustained load [kN]**
B20A-L10	20	10
B30A-L10	30	10
B40A-L10	40	10

B20P-L14.5	20	14.5
B30P-L14.5	30	14.5
B40P-L14.5	40	14.5

[a]A = cast at active end; B- cast at passive end. See Figure 1

Finally, all samples were unloaded, moved to a bending testing rig and subjected to a quasi-static four-point bending test until failure, over a span of 900 mm. The test was load controlled at a rate of 0.4 kN/min.

Measuring equipment

All samples were equipped with 3 Vishay 120±0.3% Ω foil strain gauges installed on the BFRP bars, located at midspan and supports, positioned as shown in Figure 4. Strain was continuously monitored using the VPG System 8000 data acquisition system at 1 Hz rate.

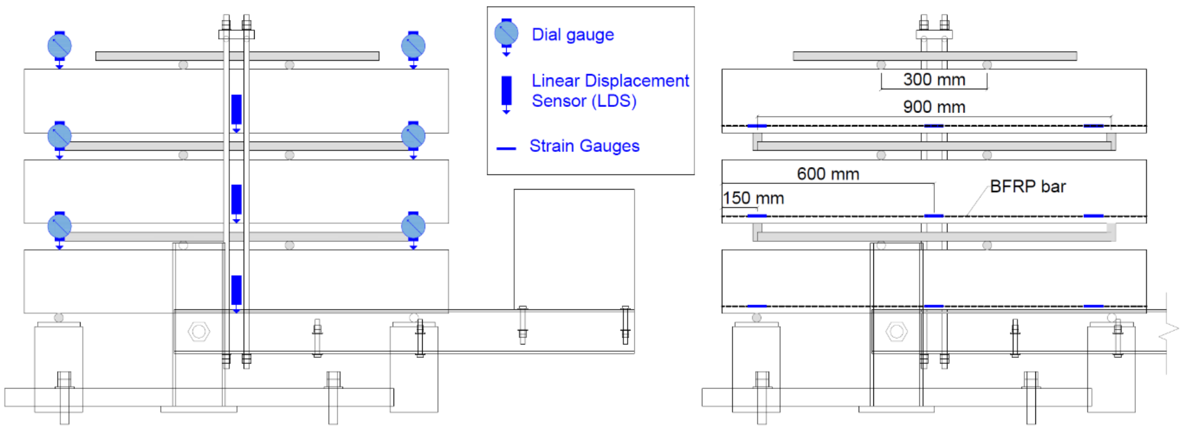

Figure 4 Positioning of the measuring equipment

During the sustained loading, the samples were equipped with loads cells, linear variable differential transformers (LVDTs) at midspan connected to the data acquisition system, and dial gauge test indicators (DTIs) at the supports. The LVDTs used were VPG model HS50, with 1-50 mm stroke, infinite resolution and <±0.1% accuracy; the DTIs used were Multitoyo Standard Dial Indicators with 0.01 mm precision. The LVDTs and dial gauges were supported by stabilised stands which were placed on the strong floor, adjacent to the testing rig, but with no physical connection to the rig. The environmental temperature was also monitored using a digital thermometer. The potential development of cracks as well as potential slippage of the bars was monitored visually at regular inspections.

During the final testing until failure, the applied load, displacements and strain on the reinforcing bars were electronically monitored and recorded. The development of cracks was monitored, traced and noted manually.

Results and discussion

The environmental temperature according to the recorded data was 20±2°C throughout all testing phases, with recorded temporary short-term variation of ±5°C. The relative humidity was also monitored to be within range of 65±3% throughout the entire period. The influence of environmental conditions on the results was therefore considered negligible and was not further analysed.

The phase before the application of the sustained loading - Strains

Data acquired during the initial monitoring phase of this experimental programme are presented in this section. Figure 5 presents the recorded strain values measured on the BFRP bars at the midspan of the beams, starting from the pretensioning of the bars, including concrete casting and curing, release of external pretension, resulting in the transfer of the prestressing force to the cured concrete, for a total period of 86 days.

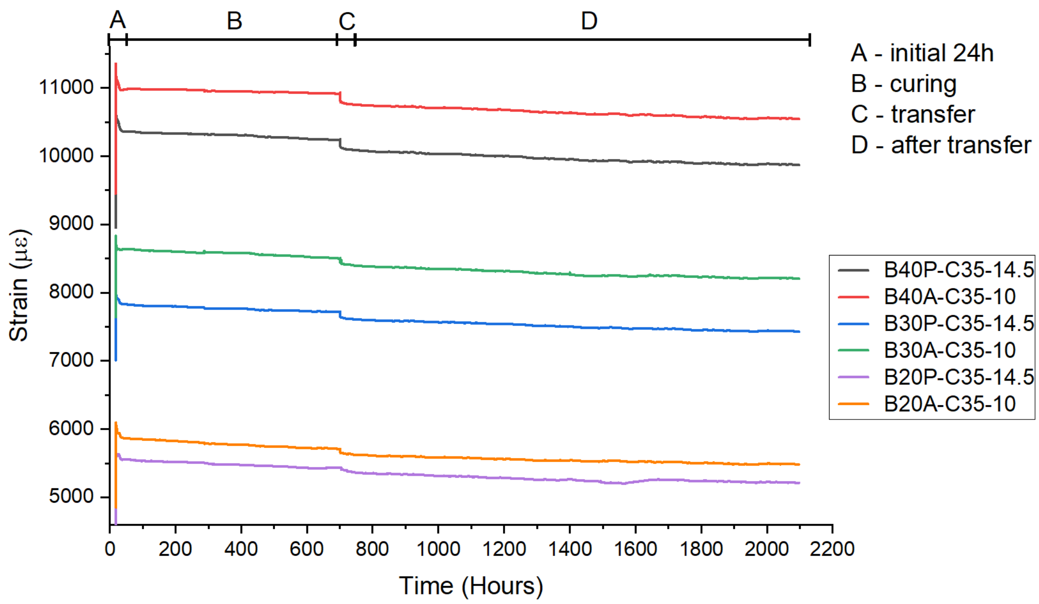

Figure 5 Recorded strain over time at midspan during the unloaded phase

As shown in Figure 5 the strain values were decreasing over the entire monitored period. The observed decrease in strain in the investigated period can likely be attributed to the combined influence of concrete shrinkage, creep and elastic deformation of concrete upon the release of prestress.

In the initial 24 h from the application of the external prestress (section A), the strain dropped by an average of 1.86%, at a rate of 0.08% per hour, possibly due to settling of the anchoring devices. Given that this phase occurs prior to the casting of the concrete, the losses can be recovered by re-adjusting of the prestress level, which has not been done during these experiments.

After the casting of the concrete, the strain decrease was more gradual, at an approximate average rate of 0.06% per day (section B). This phase represented the process of concrete curing, during which the losses were largely influenced by the shrinkage of the concrete. The value is dependent on properties of the concrete and can be limited by prudent design of the concrete mix and an appropriate curing regime to reduce shrinkage.

This was followed by a sudden drop of strain (section C), on average 0.89%, which was a result of the release of the externally applied prestress and transfer to the cured concrete. As the prestress force is transferred to the concrete element, the concrete undergoes an instantaneous elastic deformation, which results in shortening of the bars, and thus, loss of prestress. At this stage, the samples with higher initial level of prestress exhibited a higher loss during prestress transfer.

In order to estimate these losses theoretically, a numerical approach in line with Eurocode 2 can be applied. The instantaneous loss of stress due to an elastic shortening, adjusted for material properties of BFRP and loading conditions at time of release of prestress (no external load applied) can be determined by:

$$\Delta\sigma_{el} = P_{jack} \times \frac{E_{BFRP}}{E_{cm}} \times \left(\frac{1}{A_g} + \frac{e^2}{I_g}\right) \qquad (1)$$

where P_{jack} is the prestress force applied by the jack, E_{BFRP} and E_{cm} are the elastic moduli of BFRP and concrete respectively, A_g is the gross cross-sectional area, e eccentricity of the tendons and I_g second moment of inertia of the gross cross section. Young's modulus of concrete was considered as 33.34 GPa, calculated using the formula provided in EN1992-1-1 as $E_{cm} = 22 \times (f_{cm} \div 10\ MPa)^{0.3}$. The results of the calculations are plotted against the experimental results in Figure 6 as a function of the initial prestress level. A satisfactory correspondence between theoretical and experimental values can be observed, with average absolute difference of 0.2 MPa.

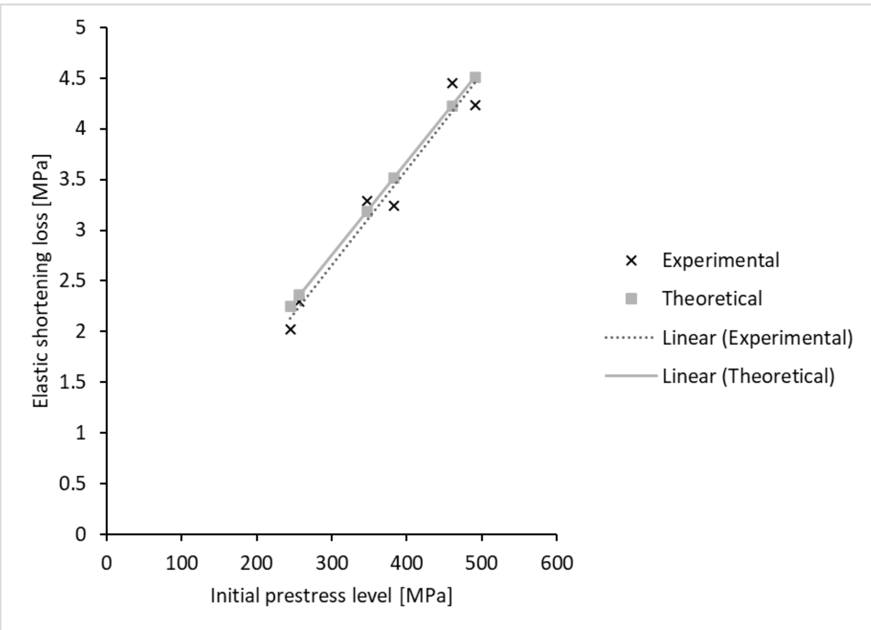

Figure 6 Comparison of EC2 based numerical and experimental values of elastic shortening loss.

The final period (section D) was characterised by a steadier rate of decrease in strains of about 0.05% per day. The dominating factors in this phase were rheological properties of concrete and the reinforcing material. At the end of the monitored period, an average total strain decrease by approximately 7.0% was observed for all samples.

Applying the approach recommended in EC2 5.10.6(2) (CEN, 1992), the losses of prestress due to creep and shrinkage of concrete can be calculated for each relevant stage, estimating the creep coefficient and shrinkage strain for the given time period and substituting for properties of BFRP in place of prestressing steel. Actual average environmental conditions (temperature, relative humidity) as well as tested concrete strength were used in the calculations to obtain the relevant creep and shrinkage coefficients using standard formulae available in EC2 (CEN, 1992). Figure 7 summarises the calculated prestress losses due to creep and shrinkage after the initial three months, comparing them with average experimentally obtained values at the corresponding stage. Based on this, the existing formulae (adjusted only for properties of BFRP) provide sufficiently accurate prediction of losses at this stage, when compared with experimental values.

Theoretically, no creep of concrete is present before the release of prestress, and shrinkage does not depend on the initially applied prestress level, therefore theoretically, the losses in this stage are the same for all samples. During stage D, creep is directly dependent on the level of prestress and is theoretically higher for samples with higher prestress level.

Finally, losses of prestress due to relaxation must be also estimated. Using the empirical formula (Equation 2) suggested by Atutis et al. 2018bAtutis et al. 2018b:

$$R=(-0.067 \times P^2+0.697 \times P+0.304) \times \ln(t)+1 \qquad (2)$$

Where R – relaxation [%]; P – level of prestress [-]; t – time [h]

the relaxation losses were calculated and superimposed on the losses due to creep and shrinkage of concrete, and elastic shortening.

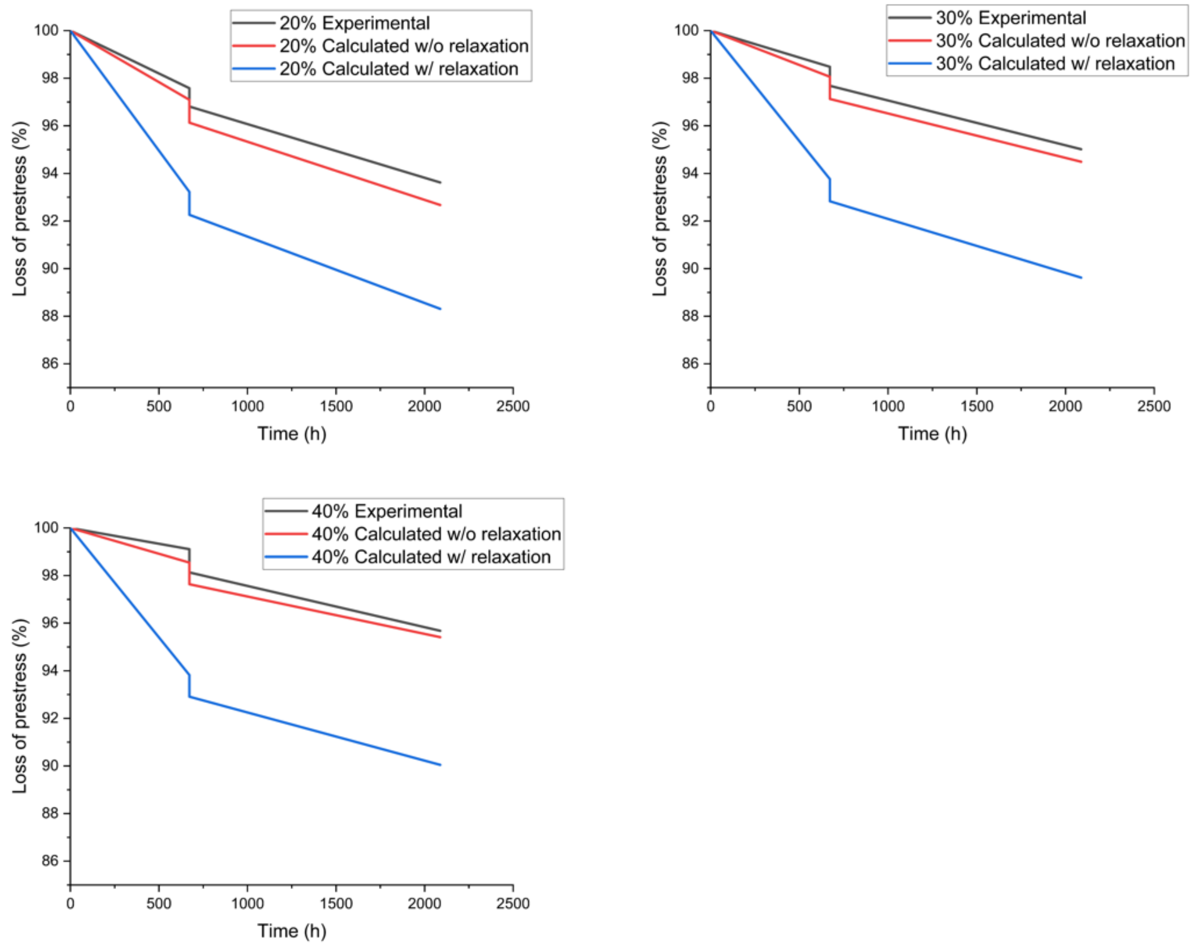

Figure 7 Theoretical and experimental decrease of strain during the unloaded testing phase.

Experimentally obtained values at relevant phases were also compared with calculated values obtained by using existing formulae available in structural codes, which provides initial confirmation that prestress losses of BFRP reinforced beams can be calculated using a similar approach to steel. Namely, losses due to creep and shrinkage of concrete, as well as elastic shortening can be sufficiently well calculated using EC2 formulae and substituting for material properties of BFRP. Due to the lower longitudinal elastic modulus of BFRP, for the same shrinkage and creep strain and elastic shortening, the losses would be lower than the same type of losses for steel.

The formula for estimating relaxation of BFRP currently available in the literature results in losses of similar magnitude as all other types of losses combined. Therefore, in order to take into account all main sources of prestress losses, relaxation of BFRP tendons will need further understanding and investigation.

Sustained Loading - Strains

Following the three months of monitoring under unloaded conditions, the samples were transferred to the sustained loading rig and the external load was applied. Strain levels in BFRP bars were acquired and recorded electronically throughout the application of the external load. Samples B20P-L14.5, B30P-L14.5 and B40P-L14.5 were loaded first up to 14.5 kN; the recorded increase in the strain readings was between 76 x 10^{-6} and 89 x 10^{-6} at the midspan zone of the bars. Then, samples B20A-L10, B30A-L10 and B40A-L10 were loaded to 10 kN, which resulted in an increase in the midspan strain between 60 x 10^{-6} and 69 x 10^{-6}. The strain increased near-linearly with the increase in the load. Figure 9 shows the results of six months of continuous strain monitoring measured at the midpoint of the BFRP bars. The initial point (day 0) of this monitoring period was taken as the day after the sustained loading had been applied. The values indicated as "ΔStrain" on the vertical axis represent recorded strain readings which were zeroed based on the initial strain at the beginning of this experimental phase. The positive sign in this figure indicates elongation.

The variation of strain during the entire period was relatively small, within the range of no more than ±50 x 10^{-6}. All samples registered final decrease of the strain in the midspan zone of the bars except for B20A-L10, which exhibited a small increase in the strain readings. The final strain decrease after 180 days was below 0.4% of the initial value for all samples, ranging from 0.04% for sample B20P-L14.5, to 0.39% for B40A-L10.

To analyse the strain change shown in Figure 9, the monitored period can be divided into three phases. The first, up to approximately 70 days, is characterised by a trend of deformation decrease, indicative of shortening of the bars. After 70 days, until approximately 150 days a slight increase in measured strain is observed for samples B40P-L14.5, B20A-L10 and B30A-L10, indicative of elongation of the bars. The remainder of samples show a tendency to maintain nearly constant deformation. In the last phase, from 150 days until end of monitoring, deformations for all samples remain nearly constant, with only temporary minor fluctuations.

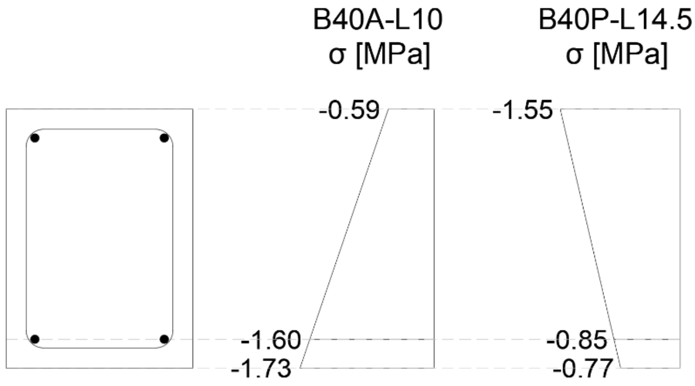

Figure 8 Stress profiles for samples B40A-L10 and B40P-L14.5. Negative sign indicates compression.

A possible explanation of any observed shortening of the bars and the corresponding reduction of strain readings is primarily due to the shrinkage and creep of concrete, under compression induced by the prestressing. Figure 8 shows the resulting stress profile due to prestress and applied stress profile; the resulting stress for all samples at the level of the bars was compression, except for samples with 20% prestress level. The greater external load resulted in higher compression at the top fibre (1.55 MPa for sample B40P-L14.5 versus 0.59 MPa for sample B40A-L10) and corresponding reduction of the compression at the bottom fibre.

The deformations due to shrinkage and creep develop throughout the life of the structure; however, they are the most pronounced in the initial period. The elongation of the bars at later stage can be explained by increase in the beam curvature due to the loss of stiffness as a result of the prestress losses.

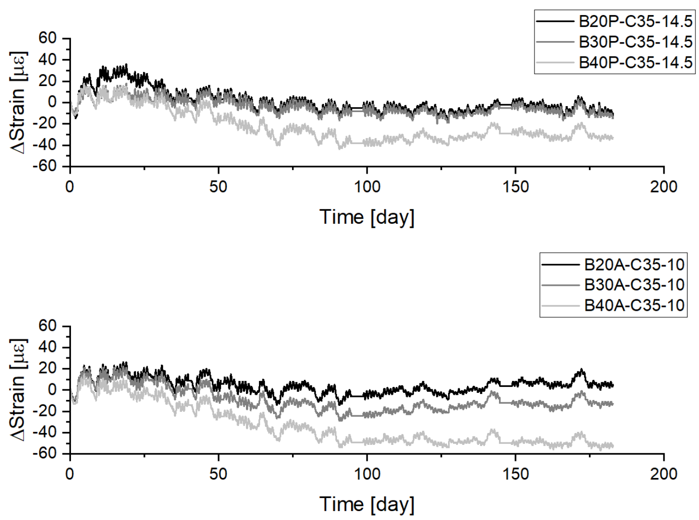

Figure 9 Strain variation at midspan during sustained loading

Figure 10 shows the recorded local change of deformation obtained from strain gauges positioned 150 mm from the edge of the beam, at the support location, presented in the same way as midspan results. There are two phases that can be defined based on the observed trend for change of deformation. In the beginning, up to approximately 70 days, the local deformation indicates shortening of the bars at a higher rate in comparison with the measured values at midspan. After 90 days, the measured deformations at supports remain nearly constant until the termination of testing, except for samples B40P-L14.5 and B40A-L10, which continued to exhibit shortening, at a slower rate than in the first phase. This can be explained by reduced creep effects as a result of continuous hardening of the concrete.

At the supports, the main factor influencing the normal stress distribution is the prestress, as the bending moments from the external load are theoretically zero. Deformational changes at the support locations are, therefore, not subject to direct influence of the external load. The governing factors influencing deformational changes at the supports are shrinkage, and creep of concrete induced by prestressing force, which gives further support to the previous conclusion regarding the behaviour at the midspan. The measured final values of relative deformation change at the support are higher than at the midspan. The creep of concrete is expected to be greater at the supports due to the higher compression stress in this zone at the level of tendon. Consecutively, shrinkage can also be higher, due to the Pickett effect.

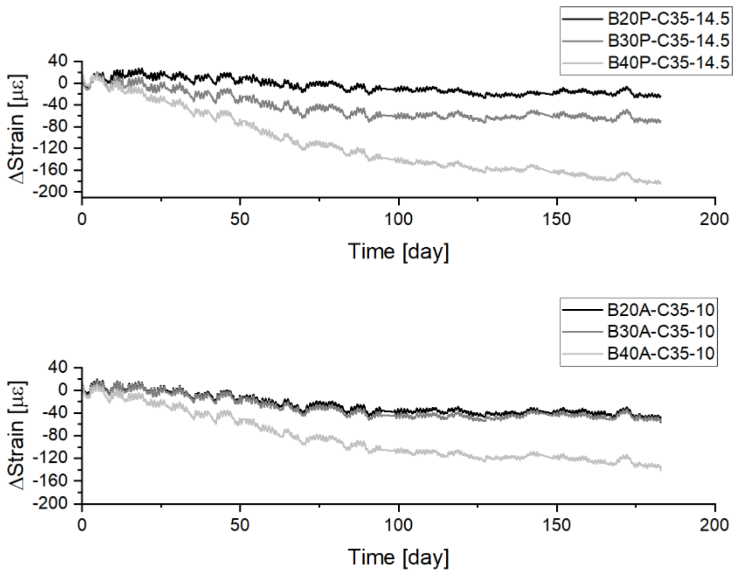

Figure 10 Strain variation over time at support under sustained loading (at 10 kN and 14.5 kN)

The measured strain decrease in 180 days at midspan, expressed in percentage of the initial strain value, was plotted against the initial strain values in order to further examine the relationship between prestress level and prestress loss (Figure 11). A line of best fit was obtained using the least square method. As shown in Figure 11, the exponential function approximates the relationship well, with coefficient of determination R^2=0.97. According to this data, the strain decrease over time rises with initial prestress level, as expected.

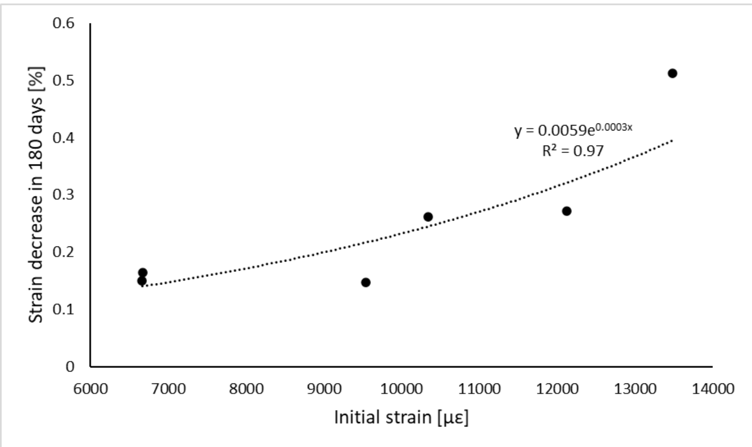

Figure 11. Percentage of strain decrease at midspan in 180 days as a function of initial strain

Summary of the strain development

During the entire long-term experimental testing programme the strain changes were recorded over the period of 9 months. The recorded changes can be analysed in the following distinct stages: curing of concrete (28 days), prestress transfer (short-term), unloaded stage after the transfer of prestress (59 days), application of sustained loading (short-term), loaded stage under sustained load (180 days) and unloading (short-term).

The change rate for the long-term periods, expressed as an average change of percentage relative to the initially applied strain per day for all six samples is shown in Figure 12, where a negative value denotes strain reduction. The strain decrease was the most intensive during the curing of concrete, while the rate was lower for the period after the transfer of prestress without external load. During the 6-month period under sustained loading, the rate was very low. This could be explained by the known rheological properties of concrete – i.e., shrinkage and creep of concrete being more intensive in the young-age rather than the mature concrete. It should also be noted that the external loading would act beneficially in the sustained loading stage with regards to strain losses, as the external load induced tension in the bars.

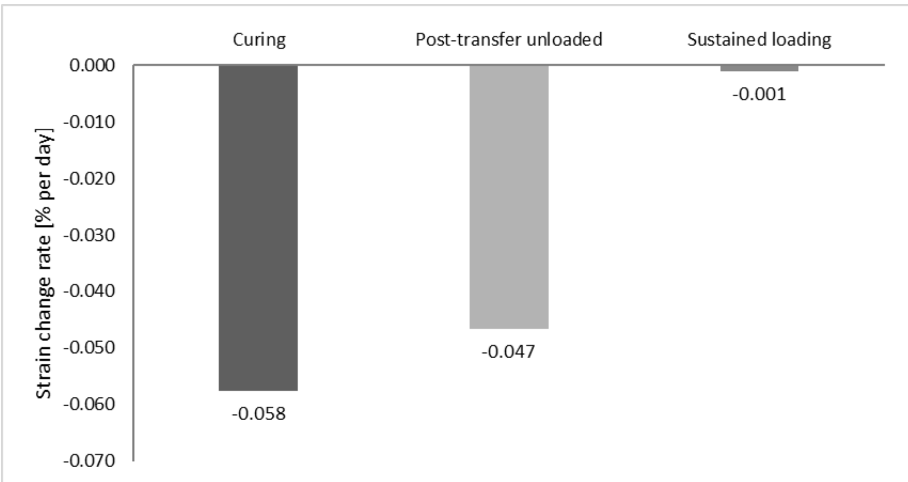

Figure 12. Long-term strain change rates for different testing periods

As previously noted, four short-term strain changes were also recorded: in the first 24 h from the application of the initial prestress, at prestress transfer, during the load application and during the unloading stage. Figure 13 shows the average total recorded strain change during each of these stages for all six samples, expressed as a percentage of the initially applied prestress, where a negative value denotes strain reduction, along with analytical predictions for corresponding stages.

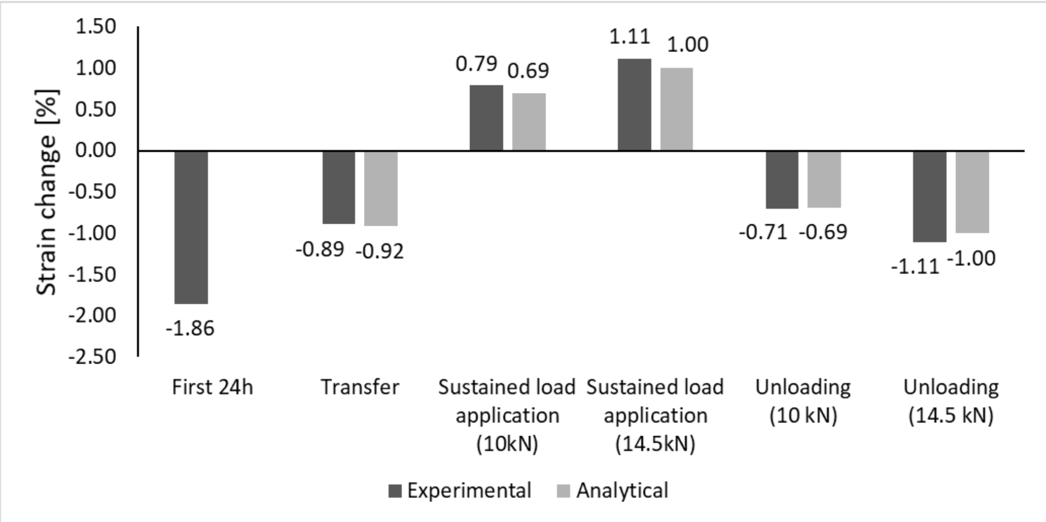

Figure 13. Strain change during short-term testing stages, experimental results and analytical predictions

Flexural behaviour under sustained loading

Instantaneous midspan deflection of a simply supported beam with two equidistant point loads, not accounting for pre-camber can be determined using:

$$\delta = \frac{23 \times P \times l^3}{648 \times E \times I} \qquad (3)$$

which equals 0.14 mm and 0.20 for 10 kN and 14.5 kN load case respectively. The experimentally measured instantaneous midspan deflection after the application of the external load was very small, not exceeding 0.2 mm for all samples. The measured value did not vary significantly with the level of prestress, which is expected, given that the applied load level falls within the elastic range of the flexural response. The value is concurrent with both deflections measured during static four-point bending tests at equal load levels, as well as with simplified numerically estimated values of 0.14 mm and 0.20 mm.

The development of deflections was followed throughout the entire period of sustained loading. No significant change of deformations (midspan deflection) was observed, below ±0.05 mm in total for all samples, which is close to the precision of the testing equipment.

The σ-stress distribution at the midspan of the beam is a resultant of the compression, introduced at the bottom by the prestressed tendons, counteracting the tension induced by the bending moment created by the external load. An increase in downwards deflection (taken as positive) under constant external load occurs as a result of rheological deformation of the material. Similarly, change of deflections in the upwards direction (taken as negative), may occur as the result of rheological deformation due to compressive (prestressing) force. The measured total change of deflections for all samples under the 14.5 kN load, regardless of the prestress level occurred in the positive (downwards) direction, indicating that the external load (applied sustained load) was the dominating force for these samples. However, for all samples under the lower, 10 kN load, regardless of their prestress level, the change of deflections was measured in the negative (upwards) direction, indication that the stress induced by external forces was counteracted in full by the prestress force.

In the investigated period, two distinctive phases were observed: from the beginning until approximately 50 days, and from 50 days until the end of testing. Change in the first 50 days of testing occurred at a rate of approximately 8×10^{-4} mm/day for samples under 14.5 kN load, and -5×10^{-4} mm/day for samples under 10 kN load. This accounted for a much larger change compared to the remainder of the period (50 days to 167 days), during which the deflections changed at a rate of approximately 4×10^{-5} mm and -1×10^{-4} mm, respectively. The much faster development of deflections in the initial one third of the testing period, followed by a much slower rate in the later period, indicates asymptotic tendency for stabilisation of the deformations, evident in the observed relatively short time period (in comparison with the life span of real structures).

The occurrence of cracks was monitored during regular daily inspections of the samples. No slippage of the bars at the ends was registered. None of the samples had any visible flexural cracks as a result of applied sustained loading for the entire duration of testing of 180 days. This is concurrent with the cracking behaviour under standard quasi-static testing for same applied load.

Flexural behaviour under final quasi-static loading until destruction.

After the completion of the sustained loading test, the samples were gradually unloaded and transferred to a reaction frame to be tested under four-point bending until destruction. After unloading, no residual midspan deflections were recorded, indicating full elastic recovery at investigated load levels.

Load vs midspan deflection curves for all samples during the final testing are shown in Figure 14. The behaviour of all pairs of samples was similar, indicating that the different levels of sustained loading have no significant influence on the flexural behaviour of the beams in this specific case. The graphs follow an approximately linear pattern up to the point that corresponds to the opening of the first flexural crack. After this point, the angle of the inclination of the load-deflection curve becomes sharper, as the deflections grow more rapidly with the increase in the load, indicating a noticeable change in the stiffness of the element. Similar behaviour continues until reaching the point of maximum load. This is immediately followed by the failure of the beam, which is characterised as brittle, occurring via rupture of the BFRP bars near the midspan for all samples.

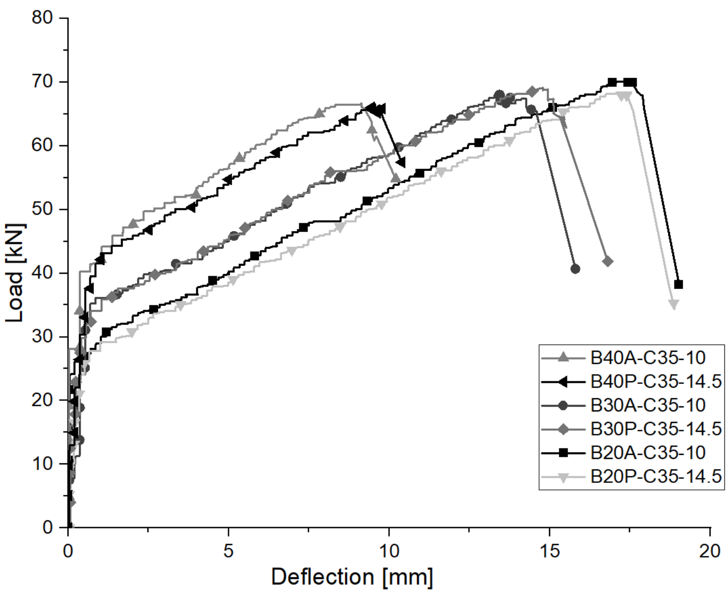

Figure 14. Load vs Deflection for all samples during final testing

Figure 15 shows a summary of the load results of the final testing. The load at failure is defined as the maximum load applied to each sample, and ranged between 66.1 kN for B40P-L14.5 to 70.1 kN for B20A-L10. The average ultimate capacity was 69.2 kN, 68.7 kN and 66.4 kN for pairs of samples prestressed to 20, 30 and 40% respectively. Based on the results it appears that increasing the prestress level results in a slightly reduced capacity of the beams. The reduction of the beams' ultimate capacity for higher levels of prestress is likely related to the higher utilisation of the bars' ultimate strain capacity introduced by the initial prestress.

SLS limit was adopted as span/250 (3.6 mm), as defined by Section 4.4.3.1(5) of Eurocode 2. As shown in the chart on Figure 15, samples with a higher level of prestressing have increased capacity according to the SLS deflection criterion.

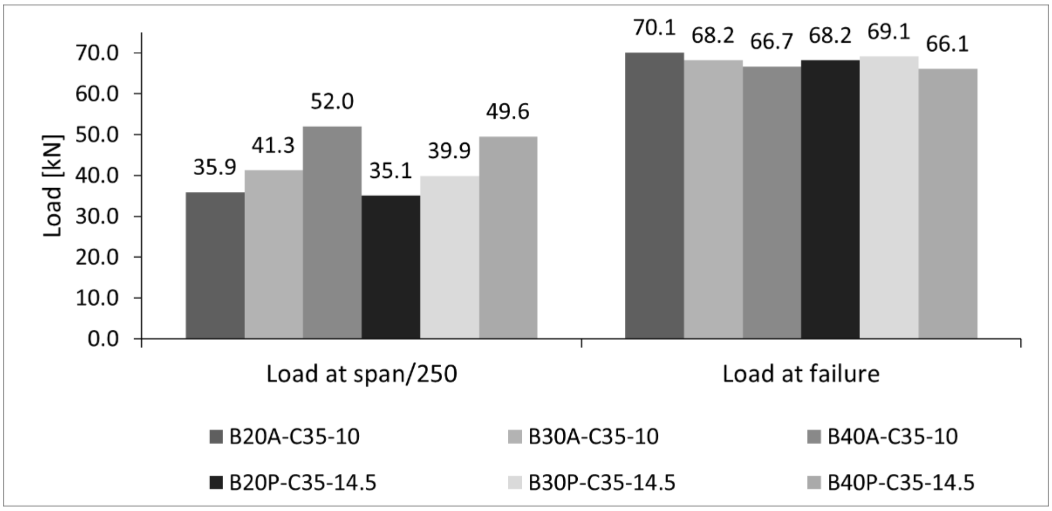

Figure 15 Summary of SLS and ULS load results of final testing

There is a clear correlation between the deflection at failure and the prestress level; increasing the prestress decreases the ultimate deflections of the beam under flexure. The highest deflection at failure was noted for sample B20A-L10 (17.4 mm), closely followed by B20P-L14.5 (17.2 mm). Compared to B20A-L10, the deflection at failure was 23% lower for B30A-L10, and 48% lower for B40A-L10. The failure of all samples was via rupture of bottom bars, as illustrated by Figure 16, which shows sample B20A-L10 at the end of testing.

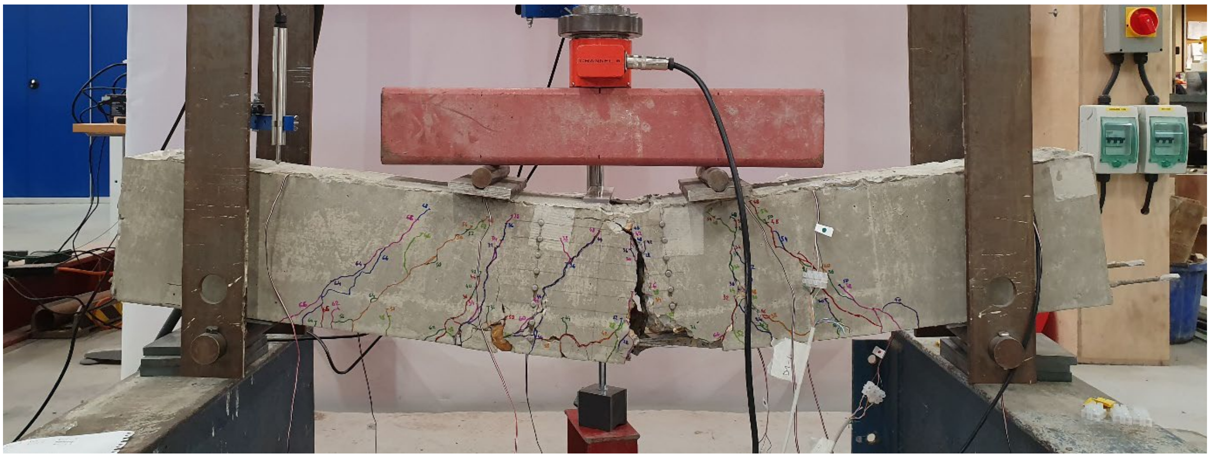

Figure 16 Sample B20A-L10 at the end of flexural testing until failure, showing rupture of the bottom reinforcement.

The appearance and development of cracks was also monitored during the testing. The first visible cracks appeared at the bottom of the samples between the applied load points as vertical flexural cracks. Figure 17 shows the applied load corresponding to the appearance of the first visible crack, as well as the total number of individual cracks at the bottom of each beam at the end of testing. The results show that the cracking pattern is related to the prestress level; the higher the prestress load, the later the first visible crack appears. Total number of cracks is also related to the prestress level; higher prestress level results in fewer flexural cracks.

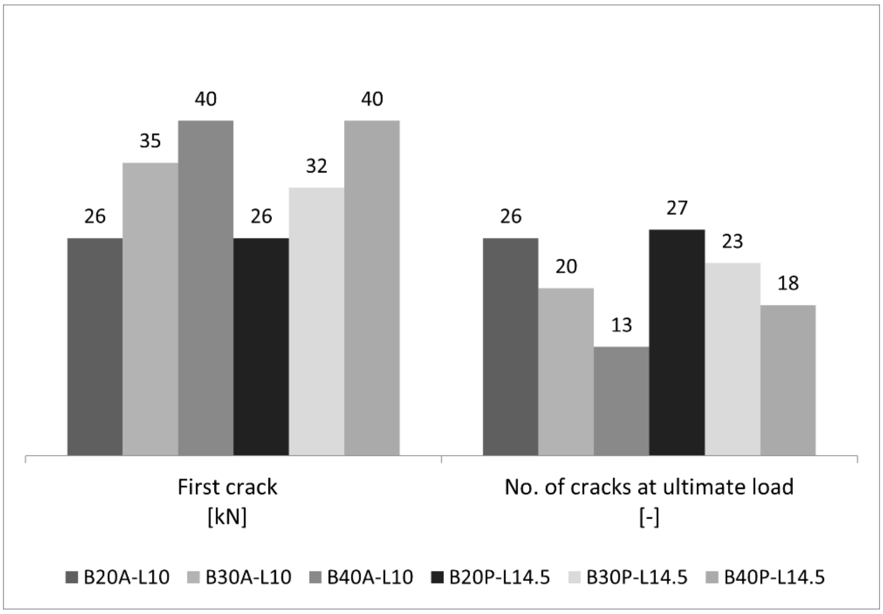

Figure 17. Crack development during final testing

To analytically estimate the flexural behaviour, structural analysis software RESPONSE2000 (Bentz, 2000) was employed to model the sectional response. The material properties of steel, concrete and BFRP were taken to be the same as explained in the methodology section, consistent with the materials used in the experiments. The beams' geometry was defined to include all reinforcement: longitudinal bottom BFRP reinforcement, top high-yield steel reinforcement and shear mild-steel reinforcement. The prestress level was defined via initial strain, as the theoretical value corresponding to 20, 30 or 40% of the ultimate strain. The model was developed for the full initial prestress value in order to assess any deviation of the experimental results from the theoretically predicted behaviour. The beams were modelled as simply supported, with a moment diagram corresponding to four-point bending and solved to obtain the moment-curvature response. The obtained diagram was then used to conduct calculations applying the moment-area approach for estimating deflections.

The resulting load vs midspan deflection curves plotted together with experimentally obtained curves are shown in Figure 18.

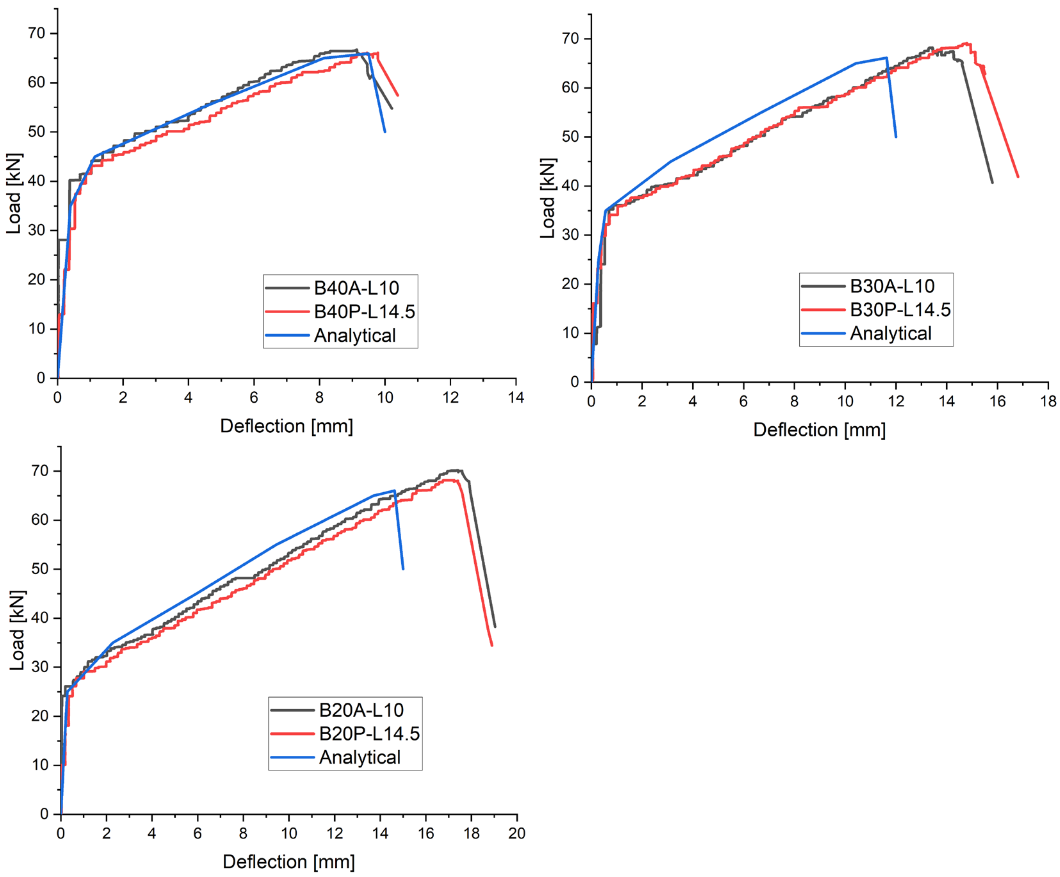

Figure 18 Comparison of experimental and analytical load vs midspan deflection curves.

A summary of main results of destructive testing, with corresponding analytically obtained values is given in Table 2. Prediction of the cracking load was accurate, whereas the deflection corresponding to the appearance of the first crack was underestimated for most beams. Furthermore, post-cracking stiffness for beams prestressed to 30% f_{tu} was overestimated by the analytical model. Nonetheless, the analytical model resulted in slightly conservative predictions of the ultimate capacity. A potential explanation for the differences, as well as a possible way for further improvement of the model could be taking into account the changes of long-term properties of both concrete and reinforcement, which have not been considered in the model presented here.

Table 2 Summary of main results of destructive testing.[1]

Sample	**Cracking load [kN]**		**Deflection at first crack [mm]**		**Ultimate load [kN]**		**Ultimate deflection [mm]**	
	Exp.	Th.	Exp.	Th.	Exp.	Th.	Exp.	Th.
B20A-L10	26	25	0.5	0.3	70.1	66.0	17.4	14.6
B30A-L10	35	35	0.8	0.6	68.2	66.2	13.4	11.6
B40A-L10	40	40	0.7	0.8	66.7	65.9	9.1	9.5

[1] Exp. – Experimental; Th. - Theoretical

B20P-L14.5	26	25	0.7	0.3	68.2	66.0	17.2	14.6
B30P-L14.5	32	35	0.9	0.6	69.1	66.2	14.8	11.6
B40P-L14.5	40	40	0.8	0.8	66.1	65.9	9.5	9.5

Conclusions

The paper presented the results of an experimental testing programme which included 6 prestressed BFRP reinforced concrete beam samples, with varying level of prestress. `Continuous monitoring of strains in the tendons allowed to estimate the losses of strain in comparison with the initial level throughout the various testing phases.

Specifically, based on the initial 3 months of strain monitoring during the unloaded phase of testing the following can be concluded:

- The reduction of strain readings during the first 24h (day 0) was the most intensive, on average of the six samples 1.86% of the initial strain. During concrete curing, from 1 to 28 days, the decrease was on average 1.58% of the initial strain.

- The instantaneous decrease due to elastic shortening during the transfer of prestress to the concrete was on average 0.86%, 0.89% and 0.91% of the initial strain, for 20%, 30% and 40% prestress level. It corresponded approximately to the values calculated using the EC2 based approach.
- The losses due to creep and shrinkage of concrete can be estimated using a similar approach to the one used for prestressed steel reinforced elements.
- The reduction of strain from the moment of transfer of prestress until 87th day was on average 2.75%, at a rate of 0.05% per day.
- The total decrease in strain in this period was on average 7.02%.

Based on 6 months period, starting from the application of sustained loading, the following conclusions can be made:

- During the load application the strains increased by an average of 83 x 10^{-6} for 14.5 kN load, and an average of 64 x 10^{-6} for 10 kN load.
- Change of strain at midspan for the sample with 40% level of prestress up to 70 days from the beginning of the testing resulted in reduction by 0.3%. The change was less pronounced for samples with 20% and 30% levels of prestress. Between 70 days and 180 days, the decrease in strain was very low.
- The total decrease in strain for the period of 6 months was on average 0.04% of the initial strain for samples with 20%, 0.14% for samples with 30%, and 0.33% with samples with 40% prestress level. The decrease in strain was higher for samples with higher initial strain.
- The total measured increase in deflections was very small, less than 0.05 mm for all samples. The dominant part of this change occurred within the initial 50 days, with very small additional increase between 50 days and the end of the sustained loading phase.

The results of final testing show that:

- The load at deflection corresponding to the SLS limit of span/250 was higher for samples with higher level of prestress

- Increase in the prestress level results in delay of the initial crack appearance, as well as in reduction of the total number of cracks at the ultimate load.

The conclusions presented here are applicable to the specific setup, materials and geometry of samples used. For further understanding of the influence of parameters other than the prestress level, e.g. bar size effect, it would be beneficial to conduct larger scale experiments of similar type.

Data availability statement

All data, models, or code that support the findings of this study are available from the corresponding author upon reasonable request.

Acknowledgements

The authors would like to express gratitude to MagmaTech Ltd for sponsoring the project by supplying RockBar BFRP reinforcement.

References

Ahmed, E. R., A. Mohamed-Amine, and M. Radhouane. 2015. "Bond Performance of Basalt Fiber-Reinforced Polymer Bars to Concrete." *Journal of Composites for Construction*, 19 (3): 04014050. American Society of Civil Engineers. https://doi.org/10.1061/(ASCE)CC.1943-5614.0000487.

Attia, K., A. el Refai, and W. Alnahhal. 2020. "Flexural Behavior of Basalt Fiber–Reinforced Concrete Slab Strips with BFRP Bars: Experimental Testing and Numerical Simulation." *Journal of Composites for Construction*, 24 (2): 04020007. American Society of Civil Engineers (ASCE). https://doi.org/10.1061/(asce)cc.1943-5614.0001002.

Atutis, M., and S. Kawashima. 2020. "Analysis of flexural concrete beams prestressed with basalt composite bars. Analytical-experimental approach." *Composite Structures*, 243. Elsevier Ltd. https://doi.org/10.1016/j.compstruct.2020.112172.

Atutis, M., J. Valivonis, and E. Atutis. 2018. "Experimental study of concrete beams prestressed with basalt fiber reinforced polymers. Part II: Stress relaxation phenomenon." *Composite Structures*, 202: 344–354. Elsevier Ltd. https://doi.org/10.1016/j.compstruct.2018.01.109.

Czigány, T. 2005. "Basalt Fiber Reinforced Hybrid Polymer Composites." *Materials Science Forum*, 473–474. https://doi.org/10.4028/www.scientific.net/MSF.473-474.59.

Dal Lago, B., S. E. Taylor, P. Deegan, L. Ferrara, M. Sonebi, P. Crosset, and A. Pattarini. 2017. "Full-scale testing and numerical analysis of a precast fibre reinforced self-compacting concrete slab pre-stressed with basalt fibre reinforced polymer bars." *Composites Part B: Engineering*, 128: 120–133. Elsevier Ltd. https://doi.org/10.1016/j.compositesb.2017.07.004.

Dhand, V., G. Mittal, K. Y. Rhee, S. J. Park, and D. Hui. 2015. "A short review on basalt fiber reinforced polymer composites." *Composites Part B: Engineering*, 73: 166–180. Elsevier Ltd. https://doi.org/10.1016/j.compositesb.2014.12.011.

Douglas, T., and F. Amir. 2015. "Performance of Concrete Beams Reinforced with Basalt FRP for Flexure and Shear." *Journal of Composites for Construction*, 19 (2): 04014036. American Society of Civil Engineers. https://doi.org/10.1061/(ASCE)CC.1943-5614.0000491.

Feng, J., Y. Zhou, P. Wang, B. Wang, J. Zhou, H. Chen, H. Fan, and F. Jin. 2017. "Experimental research on blast-resistance of one-way concrete slabs reinforced by BFRP bars under close-in explosion." *Engineering Structures*, 150: 550–561. Elsevier Ltd. https://doi.org/10.1016/j.engstruct.2017.07.074.

Gang, W., D. Zhi-Qiang, W. Xin, Z. Ying, and W. Zhi-Shen. 2015. "Prediction of Long-Term Performance and Durability of BFRP Bars under the Combined Effect of Sustained Load and Corrosive Solutions." *Journal of Composites for Construction*, 19 (3): 04014058. American Society of Civil Engineers. https://doi.org/10.1061/(ASCE)CC.1943-5614.0000517.

Gao, Y., Y. Zhou, J. Zhou, X. Kong, B. Zhang, S. Liu, J. Feng, N. Zhu, H. Fan, and F. Jin. 2020. "Blast responses of one-way sea-sand seawater concrete slabs reinforced with BFRP bars." *Construction and Building Materials*, 232. Elsevier Ltd. https://doi.org/10.1016/j.conbuildmat.2019.117254.

He, W., X. Wang, and Z. Wu. 2020. "Flexural behavior of RC beams strengthened with prestressed and non-prestressed BFRP grids." *Composite Structures*, 246. Elsevier Ltd. https://doi.org/10.1016/j.compstruct.2020.112381.

Hou, W., Z. Q. Li, W. Y. Gao, P. D. Zheng, and Z. X. Guo. 2020. "Flexural behavior of RC beams strengthened with BFRP bars-reinforced ECC matrix." *Composite Structures*, 241. Elsevier Ltd. https://doi.org/10.1016/j.compstruct.2020.112092.

Inman, M., E. R. Thorhallsson, and K. Azrague. 2017. "A Mechanical and Environmental Assessment and Comparison of Basalt Fibre Reinforced Polymer (BFRP) Rebar and Steel Rebar in Concrete Beams." *Energy Procedia*, 31–40. Elsevier Ltd.

Jason, D., K. Sara, and D. Sreekanta. 2018. "Flexural Rehabilitation and Strengthening of Concrete Beams with BFRP Composite." *Journal of Composites for Construction*, 22 (4): 04018016. American Society of Civil Engineers. https://doi.org/10.1061/(ASCE)CC.1943-5614.0000851.

Kim, Y. J., M. F. Green, and R. Gordon Wight. 2014. "2 - Prestressed fiber-reinforced polymer (FRP) composites for concrete structures in flexure: fundamentals to applications." *Advanced Composites in Bridge Construction and Repair*, Y. J. Kim, ed., 30–60. Woodhead Publishing.

Li, Z., T. Xiao, Q. Pan, J. Cheng, and S. Zhao. 2016. "Corrosion behaviour and mechanism of basalt fibres in acidic and alkaline environments." *Corrosion Science*, 110: 15–22. Elsevier Ltd. https://doi.org/10.1016/j.corsci.2016.04.019.

Lu, Z., L. Su, G. Xian, B. Lu, and J. Xie. 2020. "Durability study of concrete-covered basalt fiber-reinforced polymer (BFRP) bars in marine environment." *Composite Structures*, 234. Elsevier Ltd. https://doi.org/10.1016/j.compstruct.2019.111650.

Madotto, R., N. C. van Engelen, S. Das, G. Russo, and M. Pauletta. 2021. "Shear and flexural strengthening of RC beams using BFRP fabrics." *Engineering Structures*, 229. Elsevier Ltd. https://doi.org/10.1016/j.engstruct.2020.111606.

Meng, Q., C. Wu, J. Li, Z. Liu, P. Wu, Y. Yang, and Z. Wang. 2020. "Steel/basalt rebar reinforced Ultra-High Performance Concrete components against methane-air explosion loads." *Composites Part B: Engineering*, 198. Elsevier Ltd. https://doi.org/10.1016/j.compositesb.2020.108215.

Mirshekari, M., T. Donchev, D. Petkova, and M. Limbachiya. 2015. *INFLUENCE OF THE DEGREE OF PRESTRESSING ON THE BEHAVIOUR OF BFRP REINFORCED BEAMS*.

Mirshekari, M., T. Donchev, D. Petkova, and M. Limbachiya. n.d. *DEFORMABILITY OF PRETENSIONED PC BEAMS WITH BFRP REINFORCEMENT*.

Motwani, P., N. Perogamvros, S. Taylor, and A. Laskar. 2020. "Performance of industrial wedge-anchors for pre-stressing BFRP bars: Experimental and numerical studies." *Composite Structures*, 251. Elsevier Ltd. https://doi.org/10.1016/j.compstruct.2020.112592.

Pavlović, A., T. Donchev, D. Petkova, and M. Limbachiya. 2019a. *Initial estimate of short and long-term prestress losses of BFRP pretensioned RC beams*.

Pavlović, A., T. Donchev, D. Petkova, M. Limbachiya, and R. Almuhaisen. 2019b. "Pretensioned BFRP reinforced concrete beams: Flexural behaviour and estimation of initial prestress losses." *MATEC Web of Conferences*, 289: 09001. EDP Sciences. https://doi.org/10.1051/matecconf/201928909001.

Pavlović, A., T. Donchev, D. Petkova, and N. Staletović. 2022. "Sustainability of alternative reinforcement for concrete structures: Life cycle assessment of basalt FRP bars." *Construction and Building Materials*, 334: 127424. Elsevier. https://doi.org/10.1016/J.CONBUILDMAT.2022.127424.

Pearson, M., and T. Donchev. n.d. *Experimental Study on the Behavior of Prestressed Concrete Beams with Internal BFRP Reinforcement*.

Rafn Þórhallsson, E., B. Smari Jonsson, E. THORHALLSSON Associated Professor, and B. Smari JONSSON. n.d. *TEST OF PRESTRESSED CONCRETE BEAMS WITH BFRP TENDONS*.

Scheffler, C., T. Förster, E. Mäder, G. Heinrich, S. Hempel, and V. Mechtcherine. 2009. "Aging of alkali-resistant glass and basalt fibers in alkaline solutions: Evaluation of the failure stress by Weibull distribution function." *Journal of Non-Crystalline Solids*, 355 (52–54): 2588–2595. https://doi.org/10.1016/j.jnoncrysol.2009.09.018.

Shi, J., X. Wang, Z. Wu, and Z. Zhu. 2015. "Creep behavior enhancement of a basalt fiber-reinforced polymer tendon." *Construction and Building Materials*, 94: 750–757. Elsevier Ltd. https://doi.org/10.1016/j.conbuildmat.2015.07.118.

Singha, K. 2012. "A Short Review on Basalt Fiber." *International Journal of Textile Science*, 2012 (4): 19–28. https://doi.org/10.5923/j.textile.20120104.02.

Sokairge, H., F. Elgabbas, A. Rashad, and H. Elshafie. 2020. "Long-term creep behavior of basalt fiber reinforced polymer bars." *Construction and Building Materials*, 260. Elsevier Ltd. https://doi.org/10.1016/j.conbuildmat.2020.120437.

Suon, S., S. Saleem, and A. Pimanmas. 2019. "Compressive behavior of basalt FRP-confined circular and non-circular concrete specimens." *Construction and Building Materials*, 195: 85–103. Elsevier Ltd. https://doi.org/10.1016/j.conbuildmat.2018.11.039.

Thorhallsson, E., and S. Hlifar Gudmundsson. n.d. *TEST OF PRESTRESSED BASALT FRP CONCRETE BEAMS WITH AND WITHOUT EXTERNAL STIRRUPS*.

Wang, X., J. Shi, J. Liu, L. Yang, and Z. Wu. 2014. "Creep behavior of basalt fiber reinforced polymer tendons for prestressing application." *Materials and Design*, 59: 558–564. Elsevier Ltd. https://doi.org/10.1016/j.matdes.2014.03.009.

Wei, B., H. Cao, and S. Song. 2010. "Tensile behavior contrast of basalt and glass fibers after chemical treatment." *Materials and Design*, 31 (9): 4244–4250. https://doi.org/10.1016/j.matdes.2010.04.009.

Wei, B., H. Cao, and S. Song. 2011. "Degradation of basalt fibre and glass fibre/epoxy resin composites in seawater." *Corrosion Science*, 53 (1): 426–431. https://doi.org/10.1016/j.corsci.2010.09.053.

Wu, G., X. Wang, Z. Wu, Z. Dong, and G. Zhang. 2014. "Durability of basalt fibers and composites in corrosive environments." *Journal of Composite Materials*, 49 (7): 873–887. SAGE Publications Ltd STM. https://doi.org/10.1177/0021998314526628.

Xin, W., S. Jianzhe, W. Zhishen, and Z. Zhongguo. 2016. "Fatigue Behavior of Basalt Fiber-Reinforced Polymer Tendons for Prestressing Applications." *Journal of Composites for Construction*, 20 (3): 04015079. American Society of Civil Engineers. https://doi.org/10.1061/(ASCE)CC.1943-5614.0000649.

Younes, T., A. Al-Mayah, and T. Topper. 2017. "Fatigue performance of prestressed concrete beams using BFRP bars." *Construction and Building Materials*, 157: 313–321. Elsevier Ltd. https://doi.org/10.1016/j.conbuildmat.2017.09.086.

Zhi-Qiang, D., W. Gang, Z. Xiao-Ling, and L. Jin-Long. 2018. "Long-Term Bond Durability of Fiber-Reinforced Polymer Bars Embedded in Seawater Sea-Sand Concrete under Ocean Environments." *Journal of Composites for Construction*, 22 (5): 04018042. American Society of Civil Engineers. https://doi.org/10.1061/(ASCE)CC.1943-5614.0000876.

Zhou, Q., H. guang He, S. feng Liu, X. shuo Chen, Z. xun Tang, Y. Liu, Z. yu Qiu, S. sen Li, H. Wang, Y. zhi Zhou, J. nan Zhou, H. lin Fan, and F. nian Jin. 2021. "Blast resistance evaluation of urban utility tunnel reinforced with BFRP bars." *Defence Technology*, 17 (2): 512–530. China Ordnance Industry Corporation. https://doi.org/10.1016/j.dt.2020.03.015.

Zoghi, M. (Ed.). 2013. *The International Handbook of FRP Composites in Civil Engineering*. CRC Press.